Supplement of Geosci. Model Dev., 17, 1525–1542, 2024
https://doi.org/10.5194/gmd-17-1525-2024-supplement

Geoscientific
Model Development
Open Access

Supplement of

Quantifying wildfire drivers and predictability in boreal peatlands using a two-step error-correcting machine learning framework in TeFire v1.0

Rongyun Tang et al.

Correspondence to: Mingzhou Jin (jin@utk.edu) and Jiafu Mao (maoj@ornl.gov)

S1. Data and Validation Metrics

S1.1 Data List

Table S1 Data information for the response variables and explanatory variables

Groups	Variables	Datasets	Time Span and Resolution	Spatial Resolution	Citations
Response variables					
Fire Impacts	Burned area (BA)	GFED4.1s, FireCCI5.1	1997-2016, monthly	0.25°x0.25°	Chuvieco et al., 2018; Randerson et al., 2015
	C emission	GFED4.1s	1997-2016, monthly	0.25°x0.25°	Randerson et al., 2015
	Burn date	MCD45A1, MCD64A1	2001-2018	500m	Giglio et al., 2018; Roy et al., 2008
Explanatory variables					
Atmospheric	near-surface temperature (TMP)	CRU_ts4.04	1901-2018, monthly	0.5°x0.5°	Harris et al., 2020
	near-surface temperature minimum (TMN)	CRU_ts4.04	1901-2018, monthly	0.5°x0.5°	
	near-surface temperature maximum (TMX)	CRU_ts4.04	1901-2018, monthly	0.5°x0.5°	
	diurnal temperature range (DTR)	CRU_ts4.04	1901-2018, monthly	0.5°x0.5°	
	Precipitation (PRE)	CRU_ts4.04	1901-2019, monthly	0.5°x0.5°	
	Evapotranspiration (ET)	CRU_ts4.04	1901-2018, monthly	0.5°x0.5°	
	wet day frequency (WET)	CRU_ts4.04	1901-2018, monthly	0.5°x0.5°	
	vapor pressure (VAP)	CRU_ts4.04	1901-2018, monthly	0.5°x0.5°	
	cloud cover percentage (CLD)	CRU_ts4.04	1901-2018, monthly	0.5°x0.5°	
	ground frost frequency (FRT)	CRU_ts4.04	1901-2018, monthly	0.5°x0.5°	
	Palmer Drought Severity Index (PDSI)	CRU_ts4.04	1901-2018, monthly	0.5°x0.5°	
	Saturated vapor pressure (SVP)	$6.112 \times e^{\frac{(22.46+TMP)}{(272.62+TMP)}}$	1901-2018, monthly	0.5°x0.5°	World Meteorological Organization, 2008
	relative humidity (RH)	(VAP / SVP x 100	1901-2018, monthly	0.5°x0.5°	
	Vapor pressure deficit (VPD)	SVP - VAP	1901-2018, monthly	0.5°x0.5°	
	2-m windspeed (WIN)	MERRA2	1980-2020, 1h	0.5° x 0.625°	Gelaro et al., 2017
Vegetation	GPP	Madani et al.-2020	1982-2016, monthly	0.083°x0.083°	Madani and Parazoo, 2020
	NDVI	GIMMS3g	1982-2015, monthly	0.083°x0.083°	Pinzon and Tucker, 2014

Table S1 continued

Groups	Variables	Datasets	Time Span and Resolution	Spatial Resolution	Citations
Soil	Soil moisture (SMroot and SMsurf)	GLEAM v3.3a, v3.3b, ECMWF	1980-2018, monthly	0.5x0.5	(Martens et al., 2017
	Northern Peatland	Hugelius-2020	one period	10km	(Hugelius et al., 2020
Socioeconomic	Population density (POPD)	HYDE v3.2	10000BCE - 2015CE	0.083x0.083	(Klein Goldewijk et al., 2017

S1.2 Constructed Climate Variables

$$Saturated\ vapor\ pressure(SVP) = 6.112 \times e^{\frac{(22.46 + TMP)}{(272.62+TMP)}}, \quad \text{(S1}$$

$$relative\ humidity\ (HR) = \frac{VAP}{SAP} \times 100\%, \quad \text{(S2}$$

$$vapor\ pressure\ deficit(VPD) = SVP - VAP, \quad \text{(S3}$$

The MERRA-2 2-meter wind-speed product includes the eastward windU2M and northward windV2M, whose synthetic wind-speed is calculated as:

$$Windspeed(WSP) = \sqrt{(U2M^2 + V2M^2}, \quad \text{(S4}$$

S1.3 List of Abbreviations

Table S2 List of Abbreviations

Abbreviation	Definition
ML	Machine Learning
BP	Boreal Peatland
PLFA	Phospholipid Fatty Acid
GFED	The Global Fire Emission Database
FireCCI	The Fire Climate Change Initiative
MODIS	The Moderate Resolution Imaging Spectroradiometer
CRU	The Climatic Research Unit
GIMMIS 3g	Third-generation Global Inventory Monitoring and Modeling System
BA	Burned Area
C	Carbon
TMP	Near-surface Temperature
TMN	Near-surface Temperature Minimum
TMX	Near-surface Temperature Maximum
DTR	Diurnal temperature range
PRE	Precipitation
ET	Evapotranspiration
WET	Wet Day Frequency
VAP	Vapor Pressure
CLD	Cloud Cover Percentage
FRT	Ground Frost Frequency
PDSI	Palmer Drought Severity Index
SVP	Saturated Vapor Pressure
RH	Relative Humidity
VPD	Vapor Pressure Deficit
WIN	2-m Windspeed
GPP	Gross Primary Productivity
SMsurf	Suface Soil Moisture
SMroot	Root Soil Moisture
NDVI	Normalized Difference Vegetation Index
POPD	Population Density
FDR	False Discovery Rate
FOR	False Omission Rate
PPV	Positive Predictive Value
NPV	Negative Predictive Value
TP	True Positive
TN	True Negative
FP	False Positive
FN	False Negative
SMOTE	Synthetic Minority Oversampling Techniques
LogR	Logistic Regression
SVMs	Support Vector Machines
BAG	Bagging
KNN	K-nearest neighbors
GNB	Gaussian Naïve Bayes
LASSO	Least Absolute Shrinkage and Selection Operator
AdaBoost	Adaptive Boosting
RF	Random Forest

Table S2 continued

GBR	Gradient Boosting
Bayes	Bayesian regression
EN	Elastic Net
Kernel	Kernel Ridge
DT	Decision tree
CBR	CatBoost
LGBR	Light Gradient boosting
XGBR	Extreme Gradient boosting

S1.4 Validation metrics

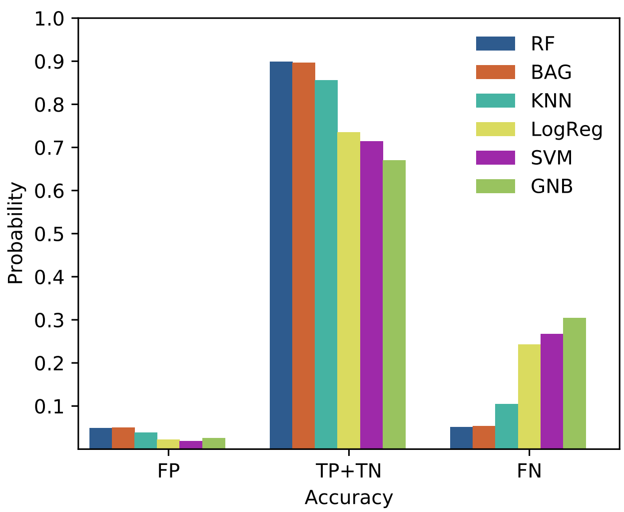

Figure S1 The histogram plots of accuracy metrices between ML predicted and observed fire/no-fire classes based on FireCCI burned area dataset. The FN stands for False Negative prediction, whose value is -1, which means that observed fires are wrongly predicted as no-fires; TP and FN stand for Ture Positive and False Negative predictions respectively, whose value is 0, meaning fires or no-fires are both correctly predicted; and FP stands for False Positive prediction, whose values is 1, meaning observed no-fire months are wrongly predicted as fire months.

Table S3 The testing evaluation metrics of simulations with different datasets; the mean value and standardized error are calculated from multiple machine learning techniques

Simulations	Data	Accuracy	Recall	Precision	AUC	PPV	FDR	FOR	NPV
all	FireCCI_BA	0.81 ± 0.08	0.71 ± 0.12	0.43 ± 0.13	0.77 ± 0.03	0.43 ± 0.13	0.57 ± 0.13	0.05 ± 0.01	0.95 ± 0.01
no-humi	FireCCI_BA	0.78 ± 0.09	0.68 ± 0.11	0.37 ± 0.11	0.74 ± 0.02	0.37 ± 0.11	0.63 ± 0.11	0.06 ± 0.01	0.94 ± 0.01
no-pre	FireCCI_BA	0.79 ± 0.09	0.70 ± 0.11	0.40 ± 0.11	0.75 ± 0.02	0.40 ± 0.11	0.60 ± 0.11	0.05 ± 0.01	0.95 ± 0.01
no-soimoi	FireCCI_BA	0.79 ± 0.09	0.68 ± 0.13	0.40 ± 0.11	0.75 ± 0.03	0.40 ± 0.11	0.60 ± 0.11	0.05 ± 0.02	0.95 ± 0.02
no-tmp	FireCCI_BA	0.79 ± 0.09	0.71 ± 0.11	0.40 ± 0.11	0.76 ± 0.02	0.40 ± 0.11	0.60 ± 0.11	0.05 ± 0.01	0.95 ± 0.01
no-tmp-hmi	FireCCI_BA	0.78 ± 0.08	0.67 ± 0.08	0.36 ± 0.10	0.73 ± 0.02	0.36 ± 0.10	0.64 ± 0.10	0.06 ± 0.01	0.94 ± 0.01
no-tmp-pre	FireCCI_BA	0.79 ± 0.08	0.70 ± 0.11	0.39 ± 0.11	0.75 ± 0.02	0.39 ± 0.11	0.61 ± 0.11	0.05 ± 0.01	0.95 ± 0.01
no-tmp-pre-hmi	FireCCI_BA	0.78 ± 0.08	0.66 ± 0.07	0.35 ± 0.10	0.73 ± 0.02	0.35 ± 0.10	0.65 ± 0.10	0.06 ± 0.01	0.94 ± 0.01
no-tmp-smo	FireCCI_BA	0.79 ± 0.09	0.70 ± 0.12	0.39 ± 0.11	0.75 ± 0.02	0.39 ± 0.11	0.61 ± 0.11	0.05 ± 0.01	0.95 ± 0.01
all	GFED_BA	0.83 ± 0.07	0.78 ± 0.03	0.53 ± 0.13	0.81 ± 0.03	0.53 ± 0.13	0.47 ± 0.13	0.05 ± 0.00	0.95 ± 0.00
no-humi	GFED_BA	0.78 ± 0.07	0.73 ± 0.06	0.45 ± 0.11	0.76 ± 0.02	0.45 ± 0.11	0.55 ± 0.11	0.06 ± 0.01	0.94 ± 0.01
no-pre	GFED_BA	0.80 ± 0.07	0.73 ± 0.08	0.48 ± 0.11	0.77 ± 0.03	0.48 ± 0.11	0.52 ± 0.11	0.06 ± 0.01	0.94 ± 0.01
no-soimoi	GFED_BA	0.80 ± 0.07	0.73 ± 0.08	0.48 ± 0.11	0.77 ± 0.02	0.48 ± 0.11	0.52 ± 0.11	0.06 ± 0.01	0.94 ± 0.01
no-tmp	GFED_BA	0.80 ± 0.07	0.74 ± 0.06	0.48 ± 0.11	0.78 ± 0.02	0.48 ± 0.11	0.52 ± 0.11	0.06 ± 0.01	0.94 ± 0.01
no-tmp-hmi	GFED_BA	0.79 ± 0.06	0.71 ± 0.05	0.46 ± 0.10	0.76 ± 0.02	0.46 ± 0.10	0.54 ± 0.10	0.07 ± 0.01	0.93 ± 0.01
no-tmp-pre	GFED_BA	0.80 ± 0.07	0.74 ± 0.07	0.48 ± 0.11	0.78 ± 0.02	0.48 ± 0.11	0.52 ± 0.11	0.06 ± 0.01	0.94 ± 0.01
no-tmp-pre-hmi	GFED_BA	0.80 ± 0.06	0.72 ± 0.03	0.47 ± 0.10	0.77 ± 0.03	0.47 ± 0.10	0.53 ± 0.10	0.06 ± 0.00	0.94 ± 0.00
no-tmp-smo	GFED_BA	0.80 ± 0.07	0.74 ± 0.06	0.47 ± 0.11	0.77 ± 0.02	0.47 ± 0.11	0.53 ± 0.11	0.06 ± 0.01	0.94 ± 0.01
all	GFED_C	0.83 ± 0.07	0.78 ± 0.03	0.53 ± 0.13	0.81 ± 0.03	0.53 ± 0.13	0.47 ± 0.13	0.05 ± 0.00	0.95 ± 0.00
no-humi	GFED_C	0.78 ± 0.07	0.73 ± 0.06	0.45 ± 0.11	0.76 ± 0.02	0.45 ± 0.11	0.55 ± 0.11	0.06 ± 0.01	0.94 ± 0.01
no-pre	GFED_C	0.80 ± 0.07	0.73 ± 0.08	0.48 ± 0.11	0.77 ± 0.03	0.48 ± 0.11	0.52 ± 0.11	0.06 ± 0.01	0.94 ± 0.01
no-soimoi	GFED_C	0.80 ± 0.07	0.73 ± 0.08	0.48 ± 0.11	0.77 ± 0.02	0.48 ± 0.11	0.52 ± 0.11	0.06 ± 0.01	0.94 ± 0.01
no-tmp	GFED_C	0.80 ± 0.07	0.74 ± 0.06	0.48 ± 0.11	0.78 ± 0.02	0.48 ± 0.11	0.52 ± 0.11	0.06 ± 0.01	0.94 ± 0.01
no-tmp-hmi	GFED_C	0.79 ± 0.06	0.71 ± 0.05	0.46 ± 0.10	0.76 ± 0.02	0.46 ± 0.10	0.54 ± 0.10	0.07 ± 0.01	0.93 ± 0.01
no-tmp-pre	GFED_C	0.80 ± 0.07	0.74 ± 0.07	0.48 ± 0.11	0.78 ± 0.02	0.48 ± 0.11	0.52 ± 0.11	0.06 ± 0.01	0.94 ± 0.01
no-tmp-pre-hmi	GFED_C	0.79 ± 0.06	0.71 ± 0.04	0.46 ± 0.10	0.76 ± 0.02	0.46 ± 0.10	0.54 ± 0.10	0.07 ± 0.00	0.93 ± 0.00
no-tmp-smo	GFED_C	0.80 ± 0.07	0.74 ± 0.06	0.47 ± 0.11	0.77 ± 0.02	0.47 ± 0.11	0.53 ± 0.11	0.06 ± 0.01	0.94 ± 0.01

Table S3 continued

Simulations	Data	Accuracy	Recall	Precision	AUC	PPV	FDR	FOR	NPV
all	MCD45A1	0.89 ± 0.06	0.89 ± 0.07	0.94 ± 0.02	0.88 ± 0.05	0.94 ± 0.02	0.06 ± 0.02	0.20 ± 0.09	0.80 ± 0.09
no-humi	MCD45A1	0.88 ± 0.04	0.89 ± 0.05	0.92 ± 0.02	0.87 ± 0.04	0.92 ± 0.02	0.08 ± 0.02	0.21 ± 0.07	0.79 ± 0.07
no-pre	MCD45A1	0.87 ± 0.05	0.88 ± 0.07	0.92 ± 0.02	0.87 ± 0.05	0.92 ± 0.02	0.08 ± 0.02	0.21 ± 0.09	0.79 ± 0.09
no-soimoi	MCD45A1	0.87 ± 0.05	0.88 ± 0.07	0.93 ± 0.02	0.87 ± 0.04	0.93 ± 0.02	0.07 ± 0.02	0.21 ± 0.08	0.79 ± 0.08
no-tmp	MCD45A1	0.87 ± 0.06	0.87 ± 0.09	0.93 ± 0.03	0.87 ± 0.05	0.93 ± 0.03	0.07 ± 0.03	0.22 ± 0.10	0.78 ± 0.10
no-tmp-hmi	MCD45A1	0.86 ± 0.07	0.86 ± 0.09	0.92 ± 0.03	0.86 ± 0.06	0.92 ± 0.03	0.08 ± 0.03	0.24 ± 0.10	0.76 ± 0.10
no-tmp-pre	MCD45A1	0.87 ± 0.06	0.87 ± 0.09	0.93 ± 0.03	0.87 ± 0.06	0.93 ± 0.03	0.07 ± 0.03	0.23 ± 0.10	0.77 ± 0.10
no-tmp-pre-hmi	MCD45A1	0.86 ± 0.07	0.86 ± 0.09	0.93 ± 0.03	0.86 ± 0.06	0.93 ± 0.03	0.07 ± 0.03	0.24 ± 0.10	0.76 ± 0.10
no-tmp-smo	MCD45A1	0.87 ± 0.06	0.87 ± 0.09	0.93 ± 0.03	0.86 ± 0.05	0.93 ± 0.03	0.07 ± 0.03	0.23 ± 0.10	0.77 ± 0.10
all	MCD64A1	0.79 ± 0.08	0.70 ± 0.09	0.41 ± 0.11	0.75 ± 0.03	0.41 ± 0.11	0.59 ± 0.11	0.06 ± 0.01	0.94 ± 0.01
no-humi	MCD64A1	0.75 ± 0.09	0.63 ± 0.11	0.36 ± 0.10	0.70 ± 0.03	0.36 ± 0.10	0.64 ± 0.10	0.07 ± 0.01	0.93 ± 0.01
no-pre	MCD64A1	0.77 ± 0.09	0.66 ± 0.11	0.38 ± 0.10	0.72 ± 0.03	0.38 ± 0.10	0.62 ± 0.10	0.07 ± 0.01	0.93 ± 0.01
no-soimoi	MCD64A1	0.76 ± 0.10	0.63 ± 0.13	0.38 ± 0.10	0.71 ± 0.03	0.38 ± 0.10	0.62 ± 0.10	0.07 ± 0.01	0.93 ± 0.01
no-tmp	MCD64A1	0.77 ± 0.09	0.65 ± 0.12	0.38 ± 0.10	0.72 ± 0.03	0.38 ± 0.10	0.62 ± 0.10	0.07 ± 0.01	0.93 ± 0.01
no-tmp-hmi	MCD64A1	0.77 ± 0.08	0.62 ± 0.09	0.37 ± 0.10	0.71 ± 0.03	0.37 ± 0.10	0.63 ± 0.10	0.07 ± 0.01	0.93 ± 0.01
no-tmp-pre	MCD64A1	0.77 ± 0.09	0.67 ± 0.09	0.39 ± 0.11	0.73 ± 0.03	0.39 ± 0.11	0.61 ± 0.11	0.06 ± 0.01	0.94 ± 0.01
no-tmp-pre-hmi	MCD64A1	0.77 ± 0.08	0.62 ± 0.08	0.37 ± 0.10	0.70 ± 0.03	0.37 ± 0.10	0.63 ± 0.10	0.07 ± 0.01	0.93 ± 0.01
no-tmp-smo	MCD64A1	0.76 ± 0.09	0.65 ± 0.10	0.37 ± 0.11	0.71 ± 0.03	0.37 ± 0.11	0.63 ± 0.11	0.07 ± 0.01	0.93 ± 0.01

Table S4 random forest performances in different simulations with different datasets

Dataset	Model	Simulation	Type	Accuracy	Recall	Precision	F1-score	AUC	PPV	FDR	FOR	NPV
FireCCI_BA	RF	all	testing	0.90	0.62	0.61	0.61	0.78	0.61	0.39	0.06	0.94
FireCCI_BA	RF	no-tmp	testing	0.89	0.60	0.56	0.58	0.77	0.56	0.44	0.06	0.94
FireCCI_BA	RF	no-pre	testing	0.89	0.60	0.55	0.57	0.76	0.55	0.45	0.06	0.94
FireCCI_BA	RF	no-humi	testing	0.88	0.57	0.53	0.55	0.75	0.53	0.47	0.06	0.94

FireCCI_BA	RF	no-soimoi	testing	0.89	0.60	0.55	0.57	0.76	0.55	0.45	0.06	0.94
FireCCI_BA	RF	no-tmp-pre	testing	0.89	0.60	0.55	0.57	0.76	0.55	0.45	0.06	0.94
FireCCI_BA	RF	no-tmp-hmi	testing	0.87	0.59	0.51	0.55	0.75	0.51	0.49	0.06	0.94
FireCCI_BA	RF	no-tmp-smo	testing	0.89	0.60	0.56	0.58	0.77	0.56	0.44	0.06	0.94
FireCCI_BA	RF	no-tmp-pre-hmi	testing	0.87	0.58	0.51	0.54	0.75	0.51	0.49	0.06	0.94
GFED_BA	RF	all	testing	0.90	0.74	0.70	0.72	0.84	0.70	0.30	0.05	0.95
GFED_BA	RF	no-tmp	testing	0.88	0.68	0.63	0.65	0.80	0.63	0.37	0.07	0.93
GFED_BA	RF	no-pre	testing	0.88	0.68	0.63	0.65	0.80	0.63	0.37	0.07	0.93
GFED_BA	RF	no-humi	testing	0.87	0.67	0.60	0.63	0.79	0.60	0.40	0.07	0.93
GFED_BA	RF	no-soimoi	testing	0.88	0.68	0.62	0.65	0.80	0.62	0.38	0.07	0.93
GFED_BA	RF	no-tmp-pre	testing	0.88	0.68	0.63	0.66	0.80	0.63	0.37	0.07	0.93
GFED_BA	RF	no-tmp-hmi	testing	0.87	0.67	0.60	0.64	0.79	0.60	0.40	0.07	0.93
GFED_BA	RF	no-tmp-smo	testing	0.88	0.68	0.63	0.65	0.80	0.63	0.37	0.07	0.93
GFED_BA	RF	no-tmp-pre-hmi	testing	0.88	0.68	0.62	0.65	0.80	0.62	0.38	0.07	0.93
GFED_C	RF	all	testing	0.90	0.74	0.70	0.72	0.84	0.70	0.30	0.05	0.95
GFED_C	RF	no-tmp	testing	0.88	0.68	0.63	0.65	0.80	0.63	0.37	0.07	0.93
GFED_C	RF	no-pre	testing	0.88	0.68	0.63	0.65	0.80	0.63	0.37	0.07	0.93
GFED_C	RF	no-humi	testing	0.87	0.67	0.60	0.63	0.79	0.60	0.40	0.07	0.93
GFED_C	RF	no-soimoi	testing	0.88	0.68	0.62	0.65	0.80	0.62	0.38	0.07	0.93
GFED_C	RF	no-tmp-pre	testing	0.88	0.68	0.63	0.66	0.80	0.63	0.37	0.07	0.93
GFED_C	RF	no-tmp-hmi	testing	0.87	0.67	0.60	0.64	0.79	0.60	0.40	0.07	0.93
GFED_C	RF	no-tmp-smo	testing	0.88	0.68	0.63	0.65	0.80	0.63	0.37	0.07	0.93
GFED_C	RF	no-tmp-pre-hmi	testing	0.87	0.66	0.60	0.63	0.79	0.60	0.40	0.07	0.93
MCD45A1	RF	all	testing	0.94	0.94	0.96	0.95	0.93	0.96	0.04	0.11	0.89

Table S4 continued

Dataset	Model	Simulation	Type	Accuracy	Recall	Precision	F1-score	AUC	PPV	FDR	FOR	NPV
MCD45A1	RF	no-tmp	testing	0.93	0.93	0.95	0.94	0.92	0.95	0.05	0.13	0.87
MCD45A1	RF	no-pre	testing	0.92	0.94	0.95	0.94	0.92	0.95	0.05	0.13	0.87
MCD45A1	RF	no-humi	testing	0.92	0.94	0.95	0.94	0.92	0.95	0.05	0.12	0.88
MCD45A1	RF	no-soimoi	testing	0.92	0.94	0.95	0.94	0.92	0.95	0.05	0.13	0.87
MCD45A1	RF	no-tmp-pre	testing	0.93	0.94	0.96	0.95	0.92	0.96	0.04	0.12	0.88
MCD45A1	RF	no-tmp-hmi	testing	0.92	0.93	0.95	0.94	0.92	0.95	0.05	0.13	0.87
MCD45A1	RF	no-tmp-smo	testing	0.92	0.93	0.95	0.94	0.92	0.95	0.05	0.13	0.87
MCD45A1	RF	no-tmp-pre-hmi	testing	0.92	0.93	0.95	0.94	0.92	0.95	0.05	0.13	0.87
MCD64A1	RF	all	testing	0.88	0.60	0.56	0.58	0.76	0.56	0.44	0.07	0.93
MCD64A1	RF	no-tmp	testing	0.87	0.55	0.53	0.54	0.74	0.53	0.47	0.08	0.92
MCD64A1	RF	no-pre	testing	0.86	0.54	0.52	0.53	0.73	0.52	0.48	0.08	0.92
MCD64A1	RF	no-humi	testing	0.86	0.52	0.52	0.52	0.72	0.52	0.48	0.08	0.92
MCD64A1	RF	no-soimoi	testing	0.86	0.52	0.52	0.52	0.72	0.52	0.48	0.08	0.92
MCD64A1	RF	no-tmp-pre	testing	0.87	0.56	0.55	0.56	0.74	0.55	0.45	0.07	0.93
MCD64A1	RF	no-tmp-hmi	testing	0.86	0.54	0.52	0.53	0.73	0.52	0.48	0.08	0.92
MCD64A1	RF	no-tmp-smo	testing	0.86	0.53	0.52	0.52	0.72	0.52	0.48	0.08	0.92
MCD64A1	RF	no-tmp-pre-hmi	testing	0.86	0.54	0.52	0.53	0.73	0.52	0.48	0.08	0.92

Table S5 validation accuracy for the ALL-simulation with SMOTE using RF

Data	Sim.	Step	Accuracy	Recall	Precision	F1-score	AUC	PPV	FDR	FOR	NPV
FireCCI_BA	ALL	testing	0.90	0.62	0.61	0.61	0.78	0.61	0.39	0.06	0.94
GFED_BA	ALL	testing	0.90	0.74	0.70	0.72	0.84	0.70	0.30	0.05	0.95
GFED_C	ALL	testing	0.90	0.74	0.70	0.72	0.84	0.70	0.30	0.05	0.95
MCD45A1	ALL	testing	0.94	0.94	0.96	0.95	0.93	0.96	0.04	0.11	0.89
MCD64A1	ALL	testing	0.88	0.60	0.56	0.58	0.76	0.56	0.44	0.07	0.93

Table S6 validation accuracy for the ALL-simulation without SMOTE using RF

Data	Sim.	Step	Accuracy	Recall	Precision	F1-score	AUC	PPV	FDR	FOR	NPV
FireCCI_BA	ALL	testing	0.91	0.42	0.77	0.54	0.70	0.77	0.23	0.08	0.92
GFED_BA	ALL	testing	0.91	0.61	0.81	0.69	0.79	0.81	0.19	0.08	0.92
GFED_C	ALL	testing	0.91	0.61	0.81	0.69	0.79	0.81	0.19	0.08	0.92
MCD45A1	ALL	testing	0.94	0.96	0.96	0.96	0.93	0.96	0.04	0.09	0.91
MCD64A1	ALL	testing	0.89	0.42	0.72	0.53	0.70	0.72	0.28	0.09	0.91

Table S7 The validation matrices of machine learning regression models with direct application

Model	Stage	MSE	MAE	R^2	Model	Stage	MSE	MAE	R^2
Ada	training	953.03	6.84	0.39	*Lasso*	training	1452.72	11.06	0.07
	testing	1068.78	6.91	0.12		testing	1141.87	10.65	0.06
Bag	training	154.47	2.38	0.90	*LGBR*	training	344.76	4.51	0.78
	testing	927.57	6.31	0.23		testing	761.45	7.03	0.37
Bayes	training	1450.62	11.26	0.07	*LinR*	training	1448.34	11.45	0.07
	testing	1142.95	10.85	0.05		testing	1146.44	11.04	0.05
CBR	training	63.89	3.13	0.96	*RF*	training	139.32	2.40	0.91
	testing	810.75	6.49	0.33		testing	928.29	6.42	0.23
DT	training	0.00	0.00	1.00	*Ridge*	training	1450.14	11.38	0.07
	testing	1841.74	7.53	-0.62		testing	1144.92	11.00	0.05
EN	training	1498.48	9.52	0.04	*Stack*	training	244.76	2.57	0.84
	testing	1159.71	8.99	0.04		testing	804.62	5.55	0.33
GBR	training	1302.99	8.55	0.17	*XGBR*	training	1550.82	6.73	0.01
	testing	1123.06	8.31	0.07		testing	1198.16	6.25	0.01
Kernel	training	1450.86	11.41	0.07					
	testing	1147.22	11.03	0.05					

S2. Research Area

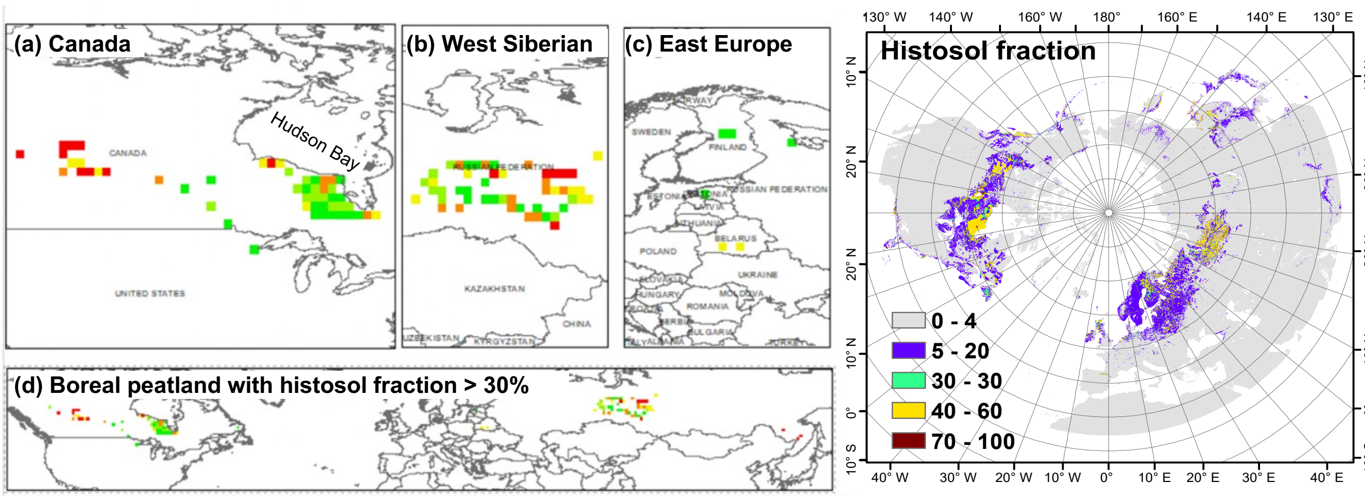

Figure S2 Research Area. Peatland fires are defined as fires happen in peatland area where histosol fraction greater than 30%d. The research area mainly locates in Hudson Bay area (a), West Siberian (b), and very few area of East Europe (c).

S3. Spatial Validation on Predicted Fire Counts

In this section, we mainly present the validating results of the predicted fire counts, spatially (in section S3) and temporally (in Section S4), with different datasets from the testing stage. These datasets include FireCCI BA, GFED BA, GFED C, MCD64A1 active fire, and MCD45A1 active fire.

S3.1 FireCCI BA

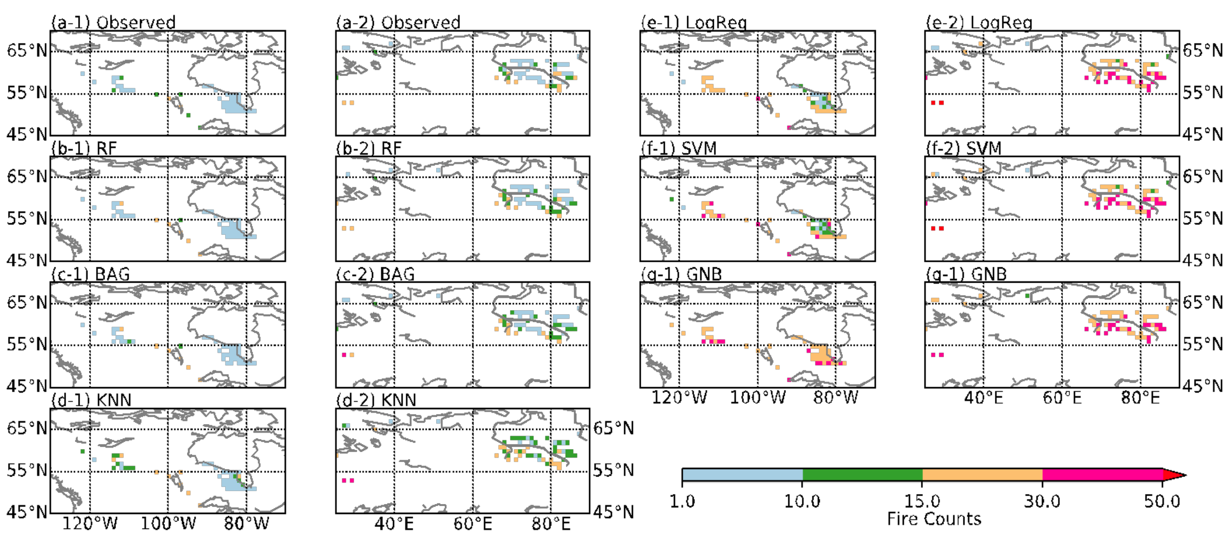

Figure S3 Spatial validation of observed and ML model predicted fire counts, based on FireCCI burned area. Subfigures in column (x-1) and (x-2) represent the data/results at Hudson Bay area (x-1) and west Siberian (x-2), respectively, where x stands for (a) observations, (b) Random Forest, (c) bagging, (d) K-nearest-neighbour, (e) logistic regression, (f) support vector machine, and (g) Gaussian Naïve Bayes model predictions.

S3.2 GFED BA

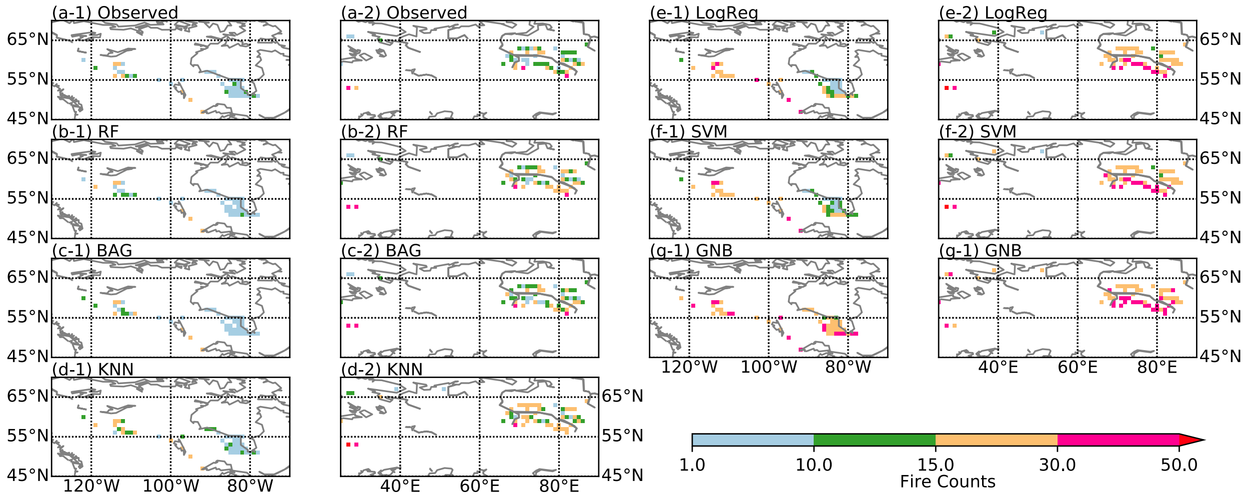

Figure S4 Spatial validation of observed and ML model predicted fire counts, based on GFED burned area. Subfigures in column (x-1) and (x-2) represent the data/results at Hudson Bay area (x-1) and west Siberian (x-2), respectively, where x stands for (a) observations, (b) Random Forest, (c) bagging, (d) K-nearest-neighbour, (e) logistic regression, (f) support vector machine, and (g) Gaussian Naïve Bayes model predictions.

GFED C emission

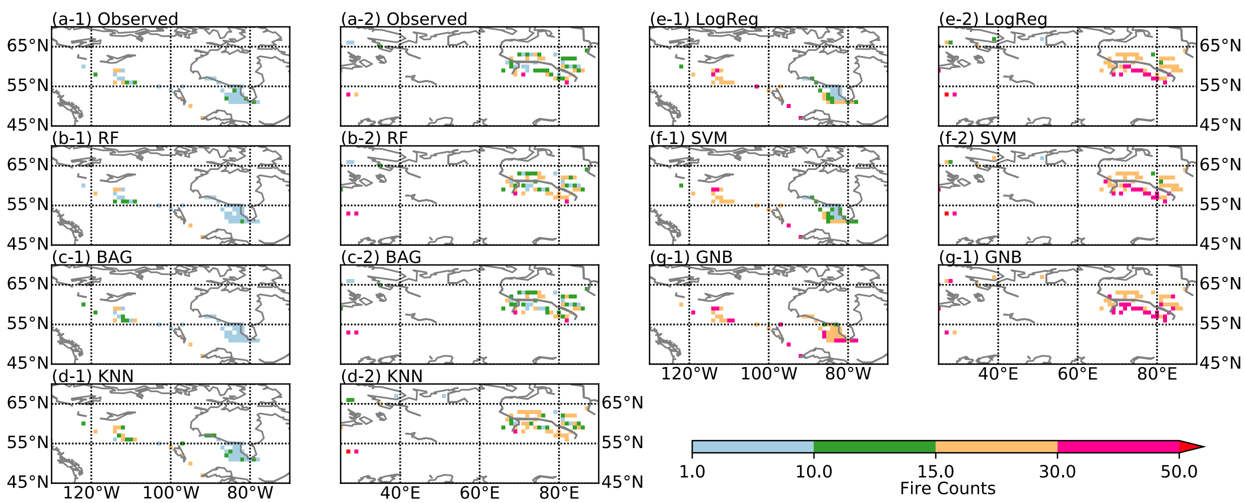

Figure S5 Spatial validation of observed and ML model predicted fire counts, based on FireCCI C emission. Subfigures in column (x-1) and (x-2) represent the data/results at Hudson Bay area (x-1) and west Siberian (x-2), respectively, where x stands for (a) observations, (b) Random Forest, (c) bagging, (d) K-nearest-neighbour, (e) logistic regression, (f) support vector machine, and (g) Gaussian Naïve Bayes model predictions.

S3.3 MCD64A1 active fire

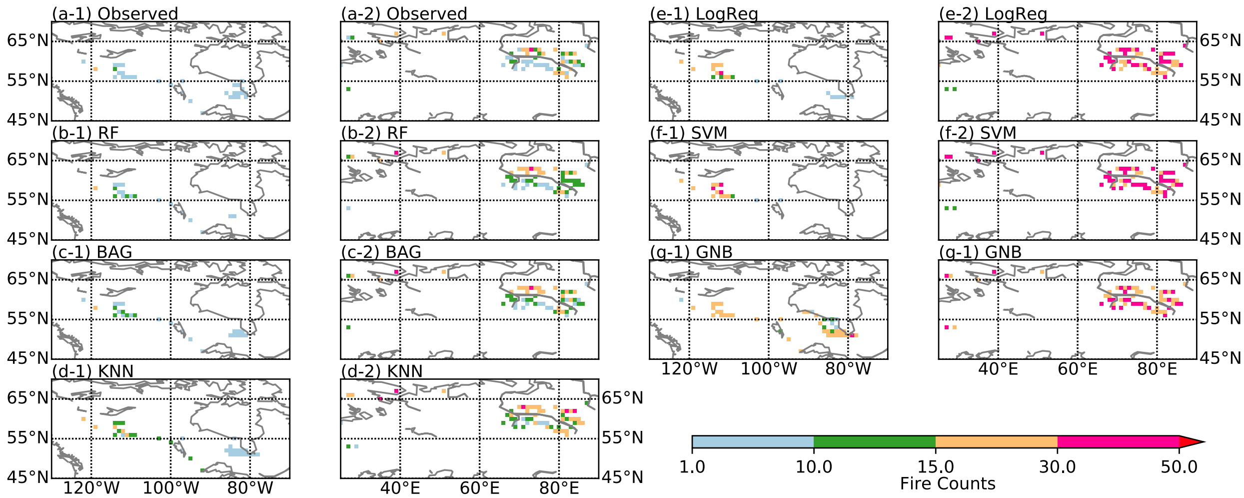

Figure S6 Spatial validation of observed and ML model predicted fire counts, based on MCD64A1 active fire. Subfigures in column (x-1) and (x-2) represent the data/results at Hudson Bay area (x-1) and west Siberian (x-2), respectively, where x stands for (a) observations, (b) Random Forest, (c) bagging, (d) K-nearest-neighbour, (e) logistic regression, (f) support vector machine, and (g) Gaussian Naïve Bayes model predictions.

S3.4 MCD45A1 active fire

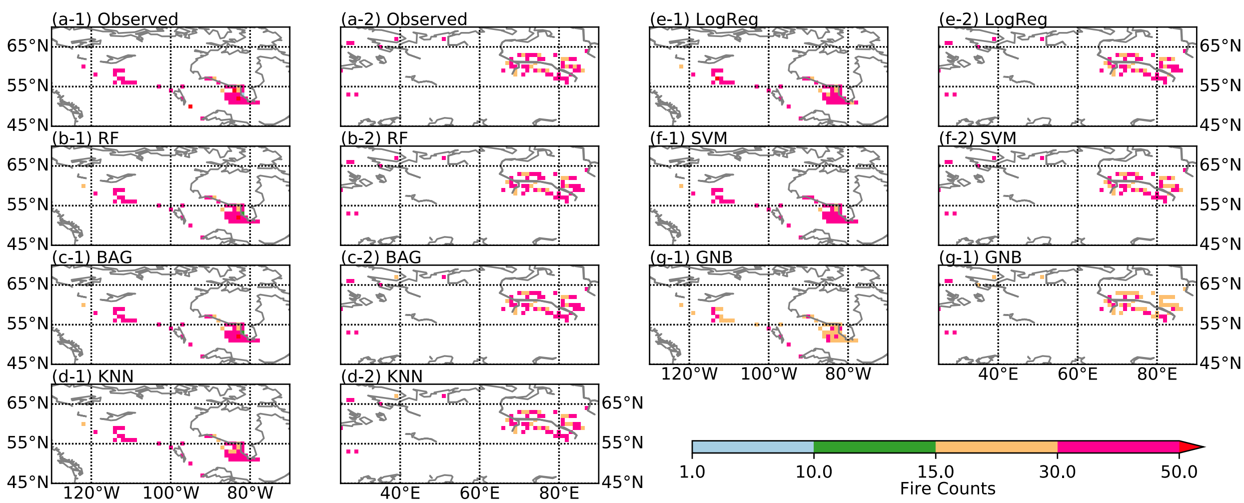

Figure S7 Spatial validation of observed and ML model predicted fire counts, based on MCD45A1 active fire. Subfigures in column (x-1) and (x-2) represent the data/results at Hudson Bay area (x-1) and west Siberian (x-2), respectively, where x stands for (a) observations, (b) Random Forest, (c) bagging, (d) K-nearest-neighbour, (e) logistic regression, (f) support vector machine, and (g) Gaussian Naïve Bayes model predictions.

S4. Temporal Validation of Predicted Fire Counts Seasonality

In this section, we mainly present the validating the seasonal distribution of predicted fire counts from the testing stage, with multiple fire datasets. These datasets include FireCCI BA, GFED BA, GFED C, MCD64A1 active fire, and MCD45A1 active fire.

S4.1 GFED BA

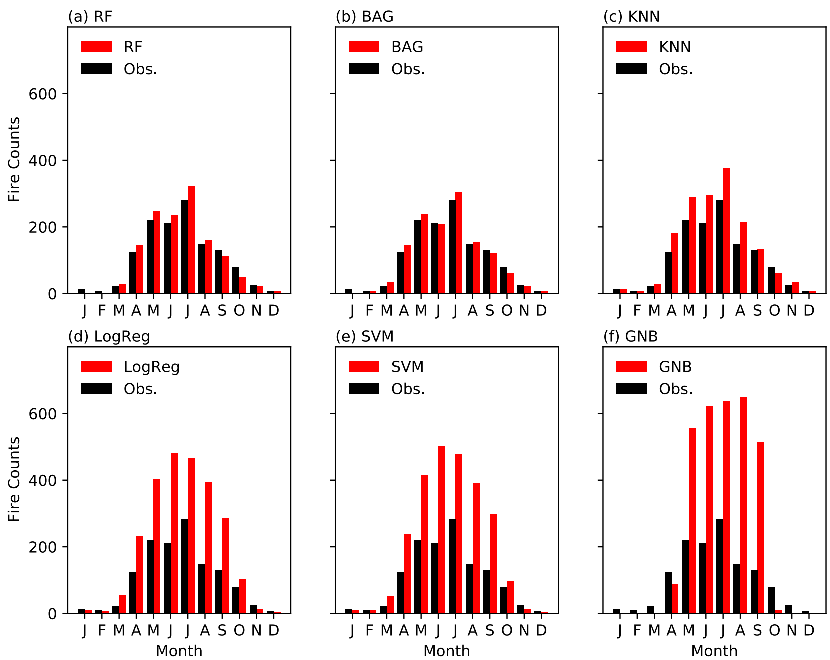

Figure S8 Temporal validation of observed and ML model predicted fire counts with GFED burned area data. Predictions (red bars) from (a) Random Forest, (b) bagging, (c) K-nearest-neighbour, (d) logistic regression, (e) support vector machine, and (f) Gaussian Naïve Bayes model are compared with observations (black bars) in seasonal distributions.

S4.2 GFED C emission

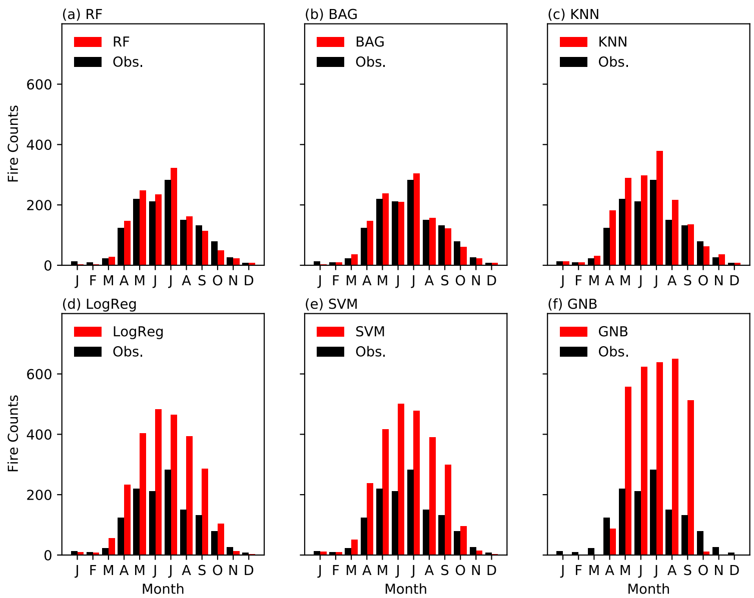

Figure S9 Temporal validation of observed and ML model predicted fire counts with GFED carbon emission. Predictions (red bars) from (a) Random Forest, (b) bagging, (c) K-nearest-neighbour, (d) logistic regression, (e) support vector machine, and (f) Gaussian Naïve Bayes model are compared with observations (black bars) in seasonal distributions.

S4.3 MCD64A1 active fire

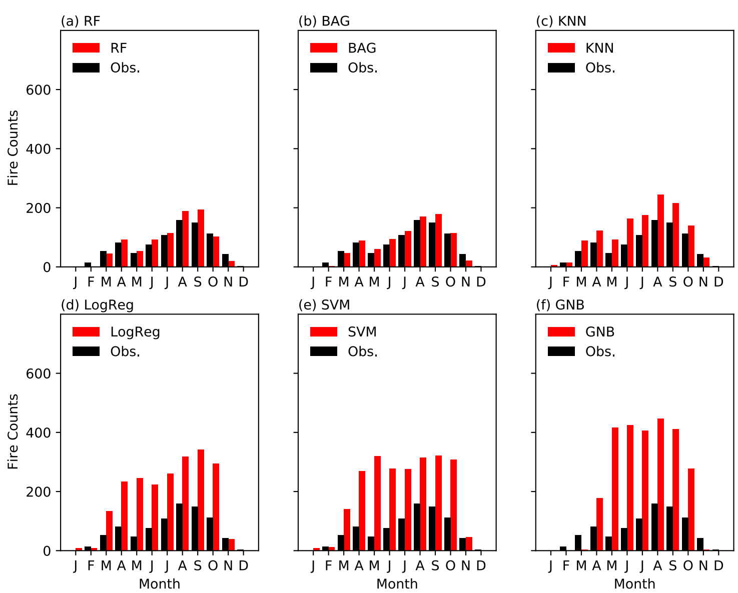

Figure S10 Temporal validation of observed and ML model predicted fire counts with MCD64A1 active fire data. Predictions (red bars) from (a) Random Forest, (b) bagging, (c) K-nearest-neighbour, (d) logistic regression, (e) support vector machine, and (f) Gaussian Naïve Bayes model are compared with observations (black bars) in seasonal distributions.

S4.4 MCD45A1 active fire

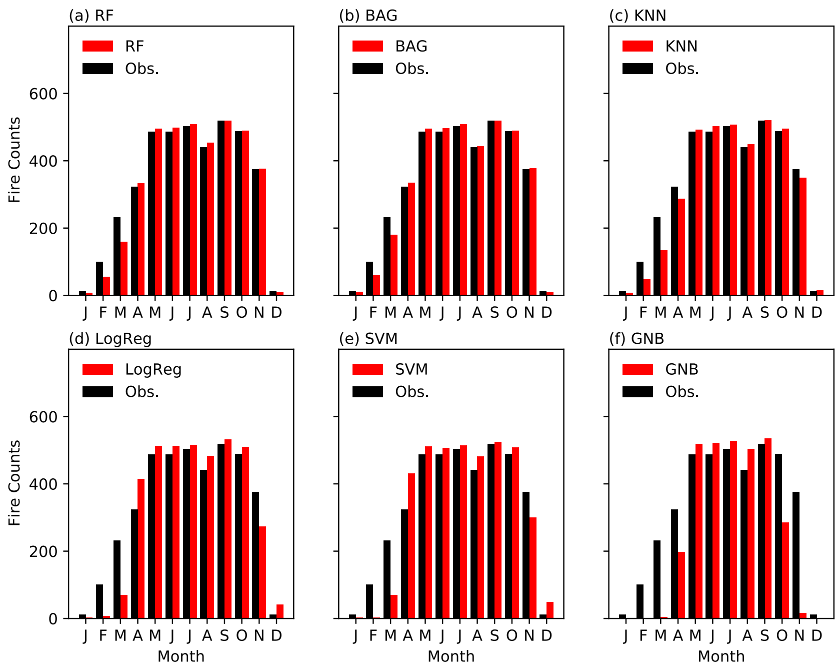

Figure S11 Temporal validation of observed and ML model predicted fire counts with MCD45A1 active fire data. Predictions (red bars) from (a) Random Forest, (b) bagging, (c) K-nearest-neighbour, (d) logistic regression, (e) support vector machine, and (f) Gaussian Naïve Bayes model are compared with observations (black bars) in seasonal distributions.

S5. Validation on Major Contributing Factors with Factor-control Simulations and Multi-datasets

In this section, we mainly present the feature importance ranking from multiple factor-controlling simulations in multi-datasets. These datasets include GFED BA, GFED C, MCD64A1 active fire, and MCD45A1 active fire. As the FireCCI-based simulation results are presented in the main text, we will not present it here.

S5.1 Feature importance from simulations based on GFED BA

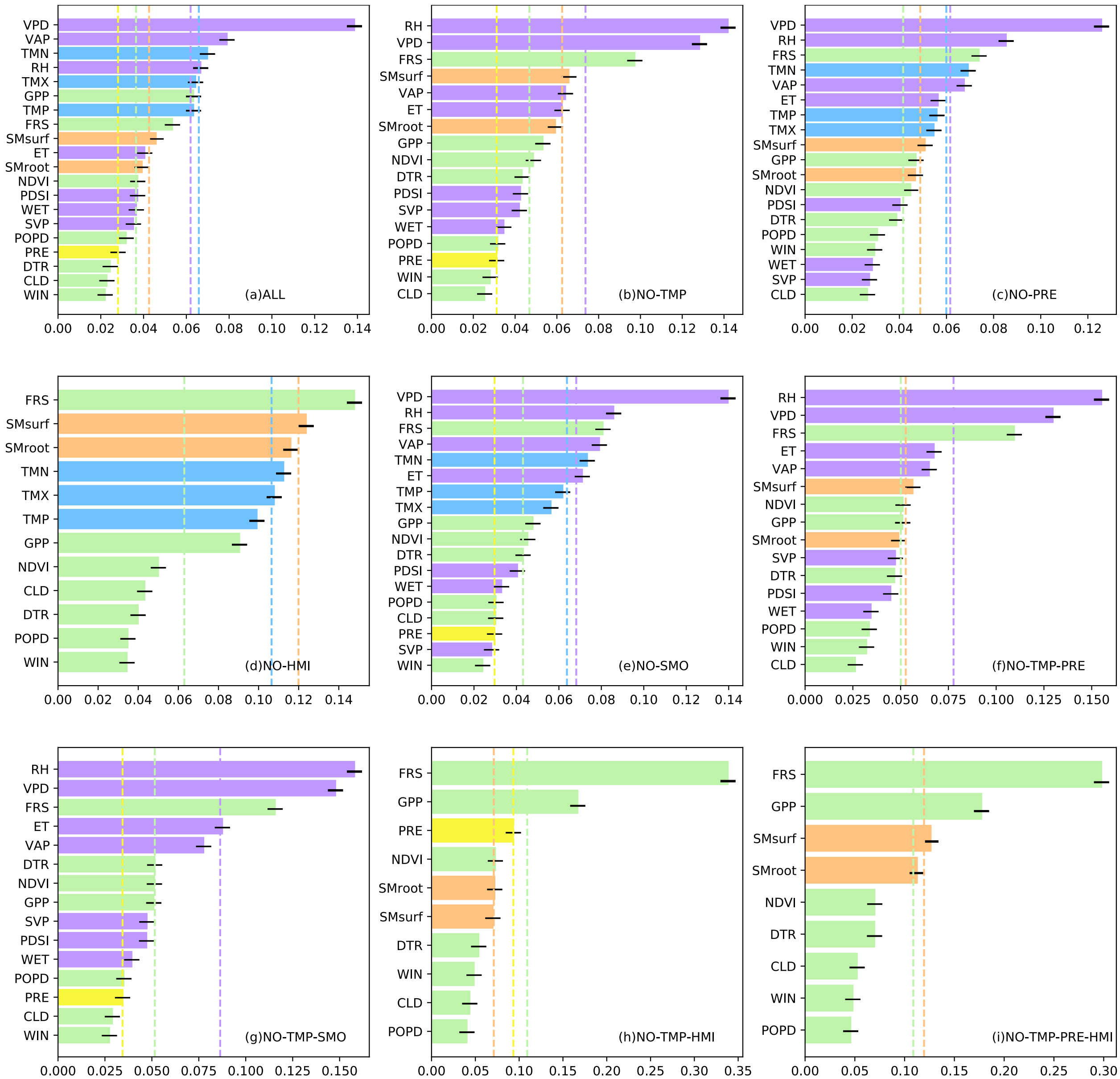

Figure S12 The synthesised factor contribution importance ranking in a range of factor-control simulations: (a) include all factor, (b) exclude features in the temperature group (marked in blue), (c) exclude features in Precipitation group(yellow), (c) exclude air-dryness group(pink), (e) exclude soil moisture group (orange), (f) exclude both temperature and precipitation,(g) exclude temperature and soil moisture, (h) exclude temperature and air-dryness, and (i) exclude temperature, precipitation, and air dryness, where the vertical lines are the mean importance of grouped features with the same colour.

S5.2 Feature importance from simulations based on GFED C emission

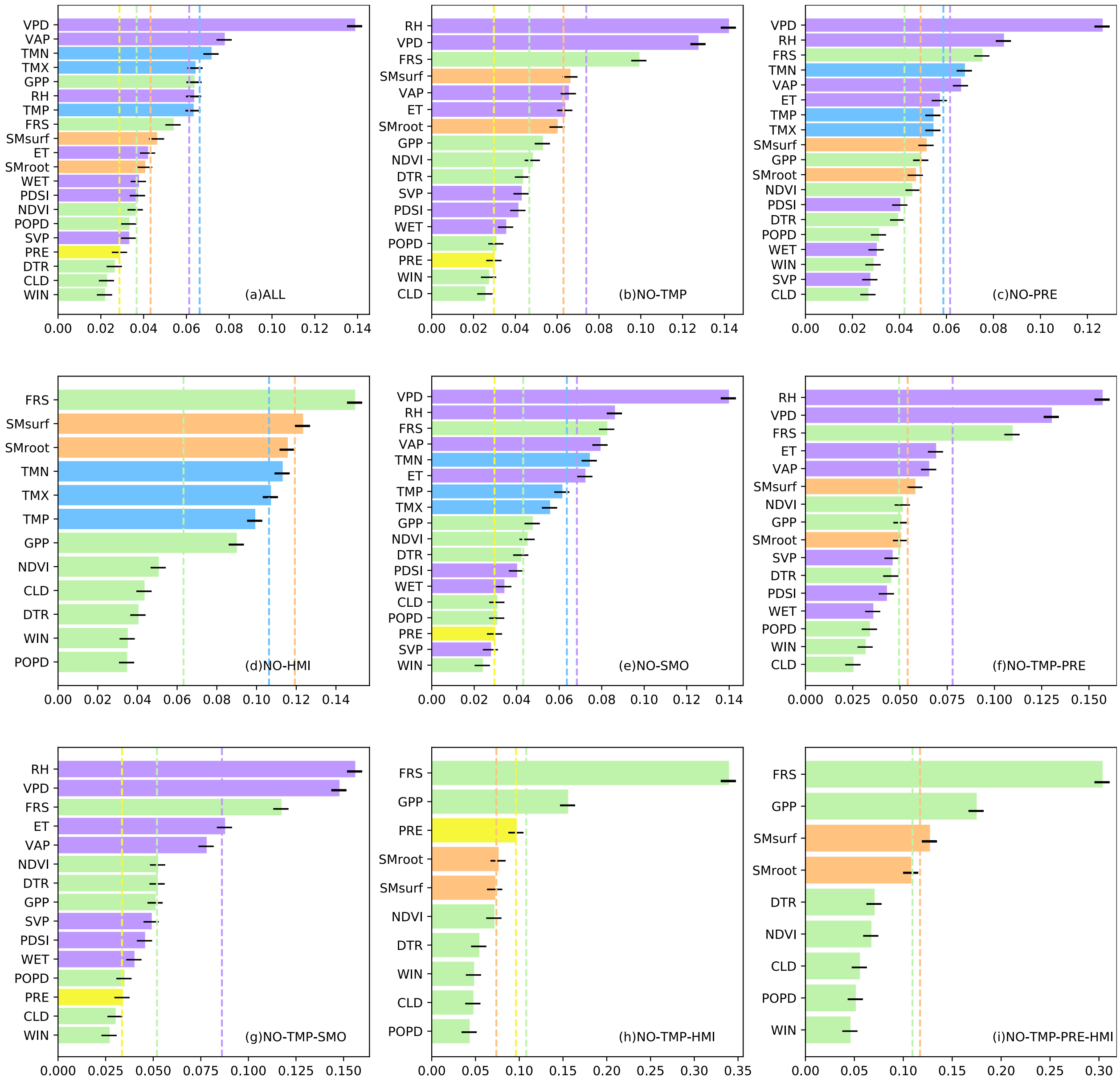

Figure S13 The synthesised factor contribution importance ranking in a range of factor-control simulations: (a) include all factor, (b) exclude features in the temperature group (marked in blue), (c) exclude features in Precipitation group(yellow), (c) exclude air-dryness group(pink), (e) exclude soil moisture group (orange), (f) exclude both temperature and precipitation,(g) exclude temperature and soil moisture, (h) exclude temperature and air-dryness, and (i) exclude temperature, precipitation, and air dryness, where the vertical lines are the mean importance of grouped features with the same colour.

S5.3 Feature importance from simulations based on MCD64A1

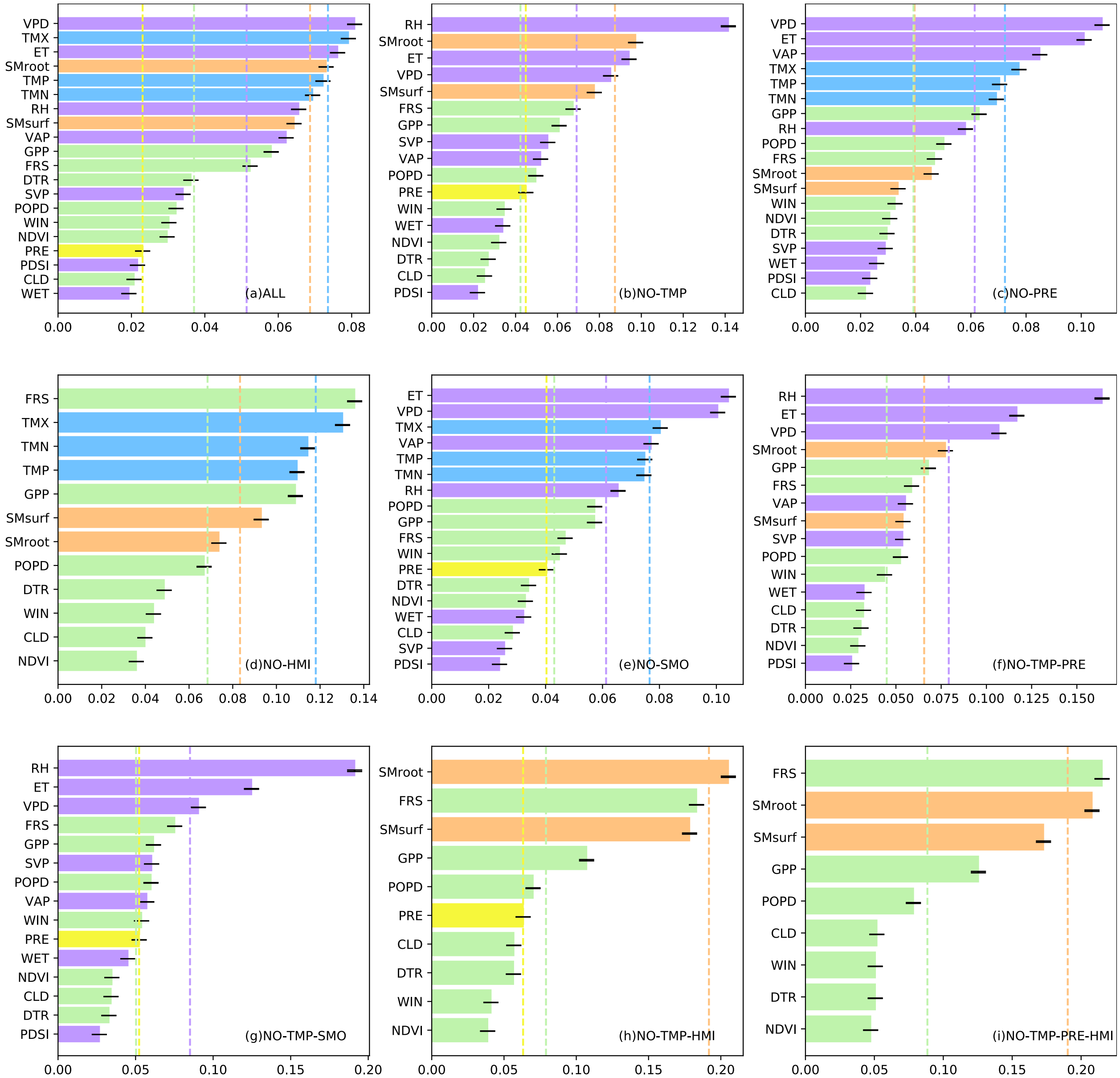

Figure S14 The synthesised factor contribution importance ranking in a range of factor-control simulations: (a) include all factor, (b) exclude features in the temperature group (marked in blue), (c) exclude features in Precipitation group(yellow), (c) exclude air-dryness group(pink), (e) exclude soil moisture group (orange), (f) exclude both temperature and precipitation,(g) exclude temperature and soil moisture, (h) exclude temperature and air-dryness, and (i) exclude temperature, precipitation, and air dryness, where the vertical lines are the mean importance of grouped features with the same colour.

S5.4 Feature importance from simulations based on MCD45A1

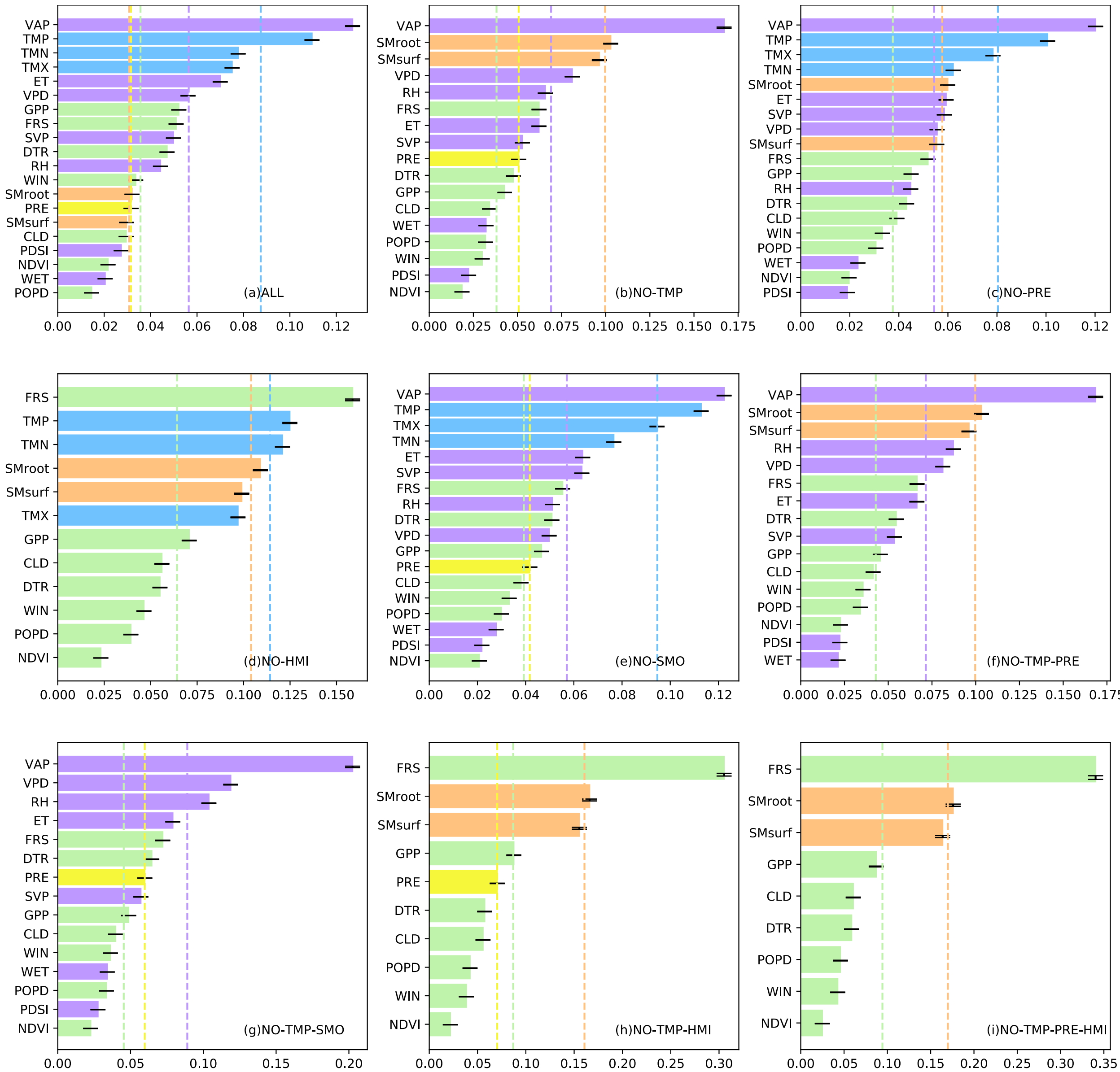

Figure S15 The synthesized factor contribution importance ranking in a range of factor-control simulations: (a) include all factor, (b) exclude features in the temperature group (marked in blue), (c) exclude features in Precipitation group(yellow), (c) exclude air-dryness group(pink), (e) exclude soil moisture group (orange), (f) exclude both temperature and precipitation,(g) exclude temperature and soil moisture, (h) excludes temperature and air-dryness, and (i) exclude temperature, precipitation, and air dryness, where the vertical lines are the mean importance of grouped features with the same color.

S6. Spatial Validation on Predicted Fire Impact Sizes

In this section, we validated the spatial distribution of predicted fire sizes either burned area or C emission from the testing stage, with multiple fire datasets. These datasets include FireCCI BA, GFED BA, and GFED C emission.

S6.1 FireCCI burned area

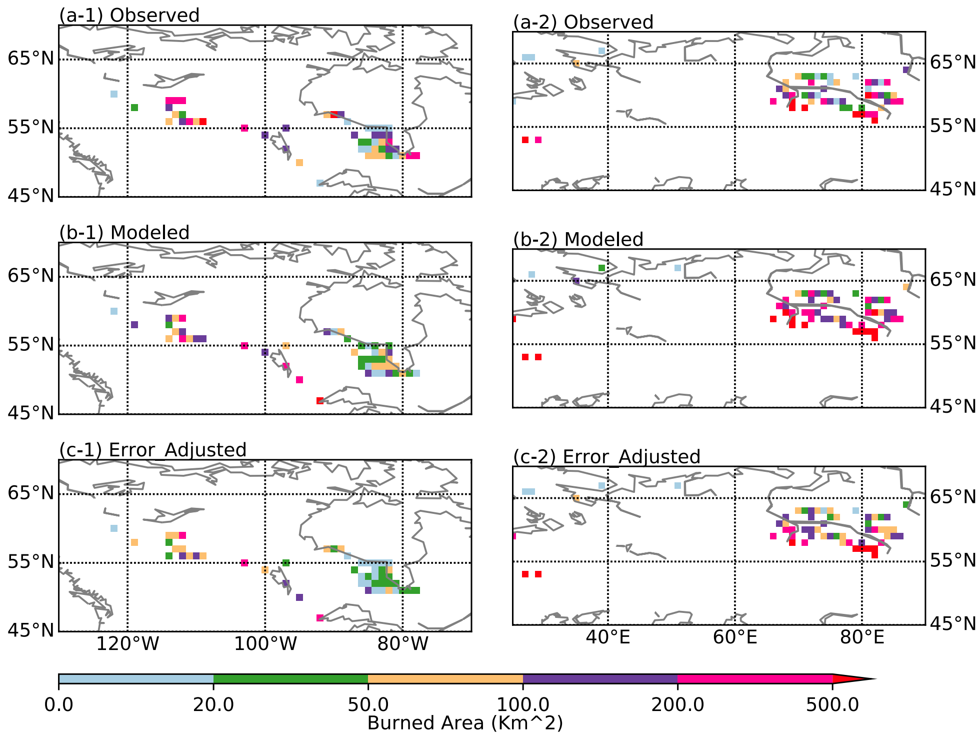

Figure S16 Spatial validation of observed, stacked machine learning predicted, and the error-adjusted burned area magnitudes, based on FireCCI burned area dataset. Subfigures in column (x-1) and (x-2) represent the data/results at Hudson Bay area (x-1) and west Siberian (x-2), respectively, where x stands for(a) observations, (b) stacked model predictions, and (c) model prediction with error-correction.

S6.2 GFED BA

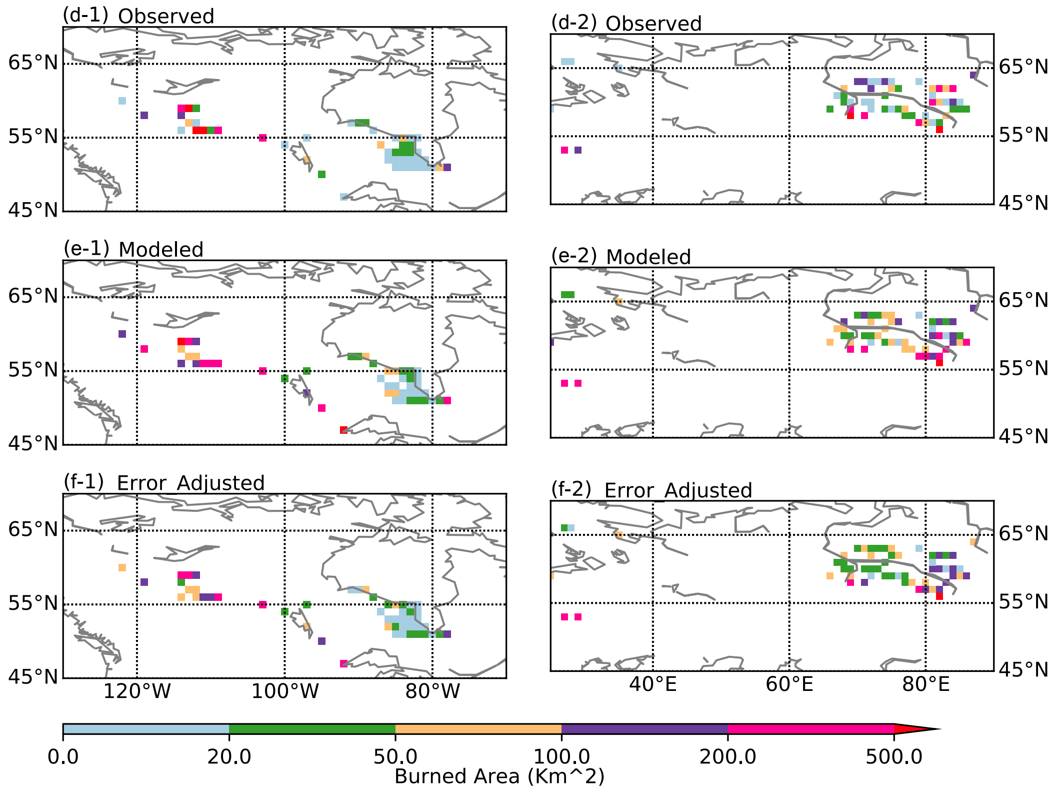

Figure S17 Spatial validation of observed, stacked machine learning predicted, and the error-adjusted burned area magnitudes, based on GFED burned area dataset. Subfigures in column (x-1) and (x-2) represent the data/results at Hudson Bay area (x-1) and west Siberian (x-2), respectively, where x stands for(a) observations, (b) stacked model predictions, and (c) model prediction with error-correction.

.

S6.3 GFED C emission

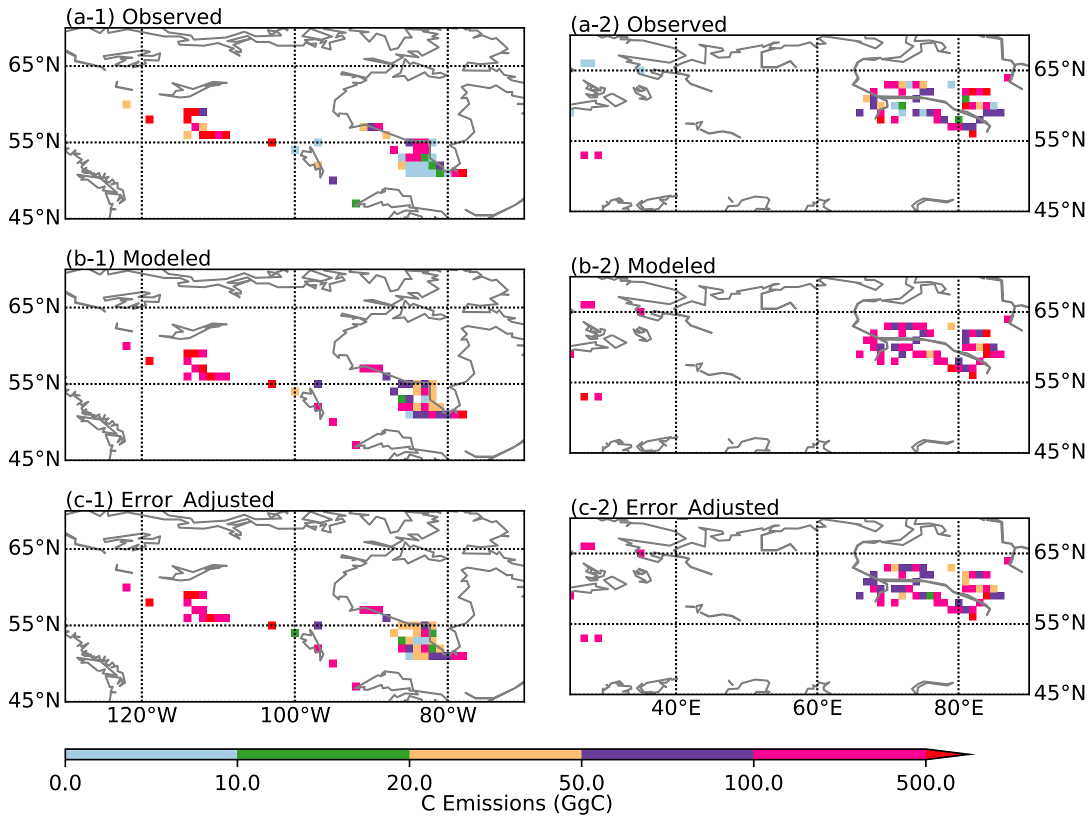

Figure S18 Spatial validation of observed, stacked machine learning predicted, and the error-adjusted burned area magnitudes, based on FireCCI burned area dataset. Subfigures in column (x-1) and (x-2) represent the data/results at Hudson Bay area (x-1) and west Siberian (x-2), respectively, where x stands for(a) observations, (b) stacked model predictions, and (c) model prediction with error-correction.

S7. Temporal Validation of Predicted Fire Impact Sizes

In this section, we validated the temporal distribution of predicted fire size, either burned area or C emission, at the testing stage with multiple fire datasets. These datasets include FireCCI BA, GFED BA, and GFED C emission.

S7.1 FireCCI burned area

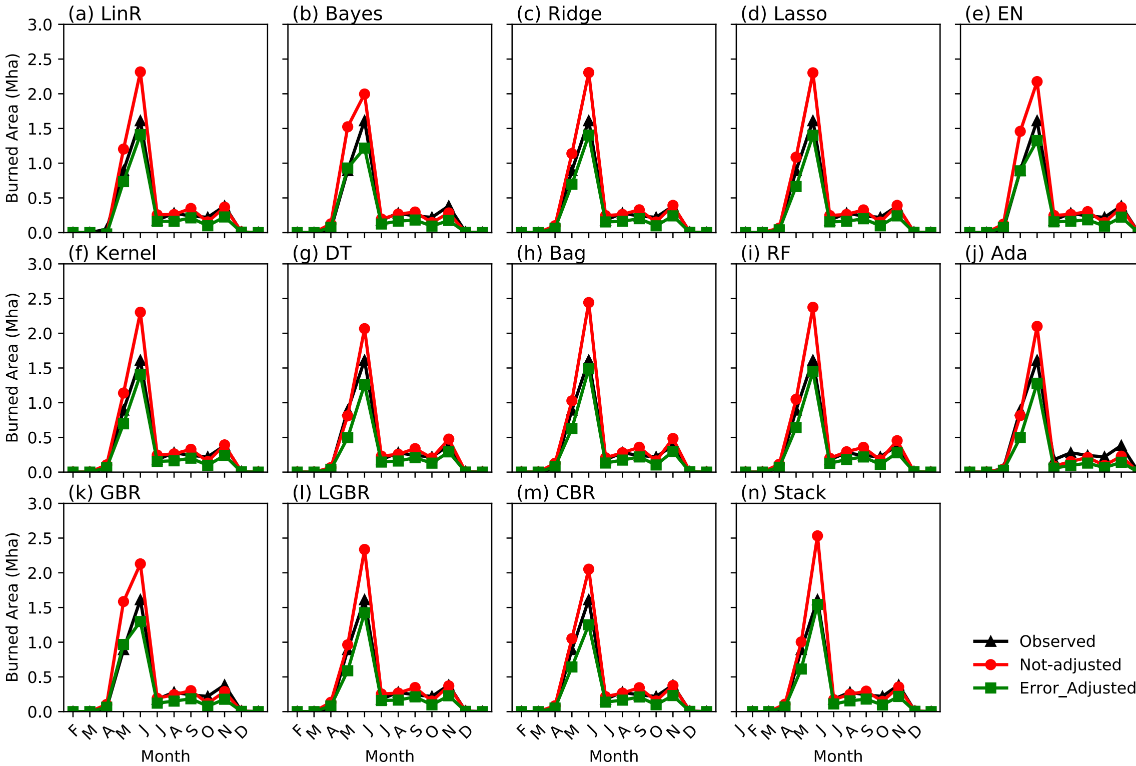

Figure S19 Seasonality of the observed, modelled, and error adjusted FireCCI burned area from multiple machine learning leaners: (a) Linear Regression; (b) Bayesian linear Regression;(c) Ridge regression; (d) Lasso regression; (e) Elastic Net; (f) Kernel ridge regression; (g) Decision tree; (h) Bagging; (i) Random forests; (j) Adaptive boosting regression; (k) Gradient boosting regression; (l) Light gradient boosting regression;(m) Cat boosting regression; and (n) stacking.

S7.2 GFED BA

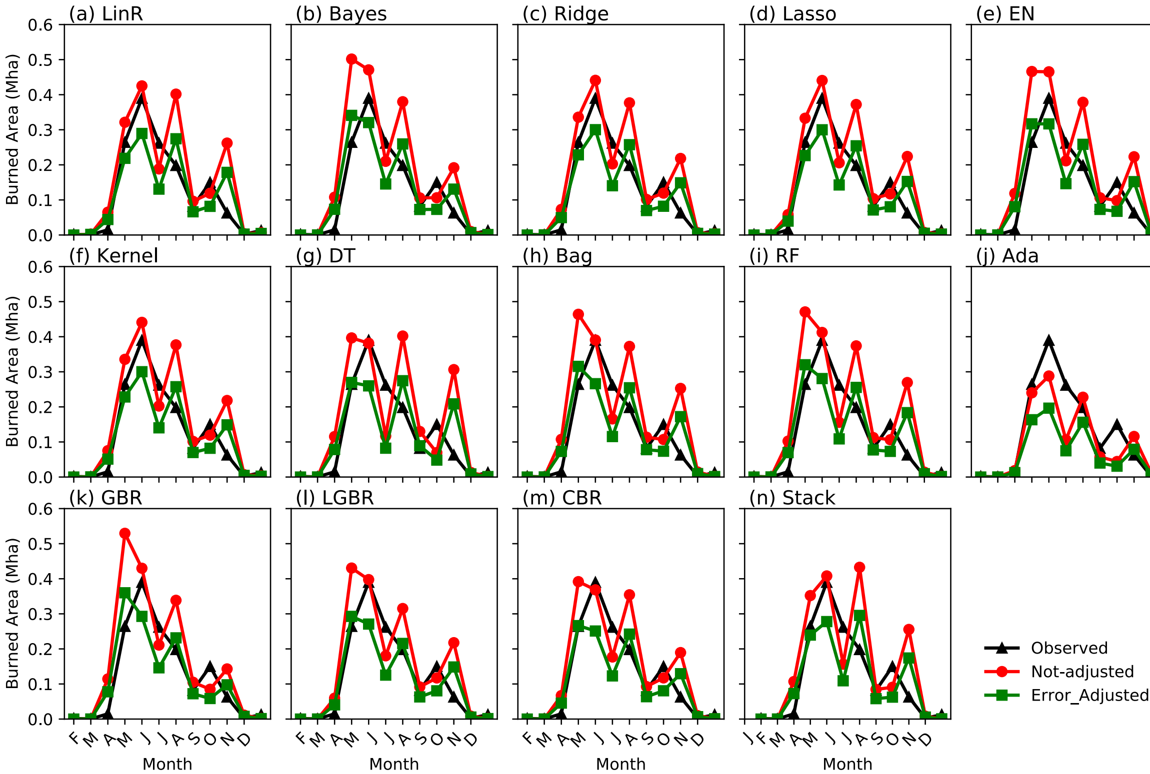

Figure S20 Seasonality of the observed, modelled, and error adjusted GFED burned area from multiple machine learning leaners: (a) Linear Regression; (b) Bayesian linear Regression;(c) Ridge regression; (d) Lasso regression; (e) Elastic Net; (f) Kernel ridge regression; (g) Decision tree; (h) Bagging; (i) Random forests; (j) Adaptive boosting regression; (k) Gradient boosting regression; (l) Light gradient boosting regression;(m) Cat boosting regression; and (n) stacking.

S7.3 GFED C emission prediction in testing set

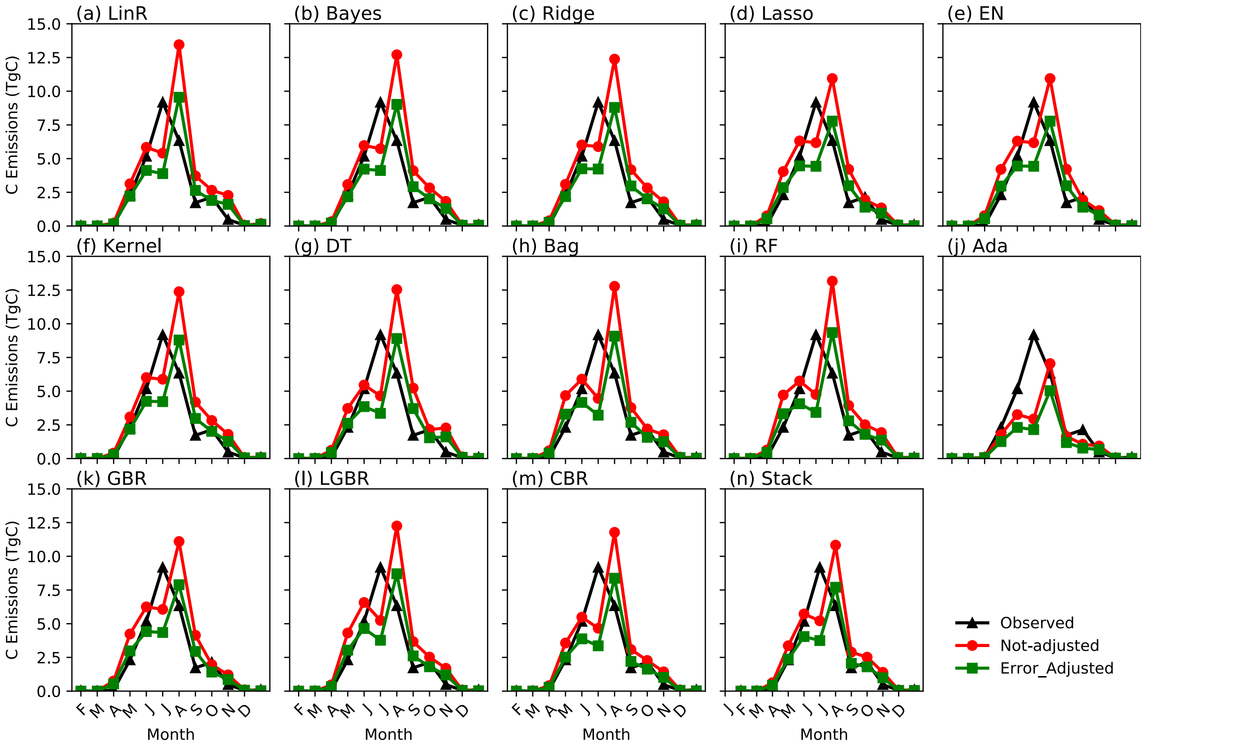

Figure S21 Seasonality of the observed, modelled, and error adjusted GFED C emission from multiple machine learning leaners: (a) Linear Regression; (b) Bayesian linear Regression;(c) Ridge regression; (d) Lasso regression; (e) Elastic Net; (f) Kernel ridge regression; (g) Decision tree; (h) Bagging; (i) Random forests; (j) Adaptive boosting regression; (k) Gradient boosting regression; (l) Light gradient boosting regression;(m) Cat boosting regression; and (n) stacking.

S8. Evaluation on the Error-correcting Effects

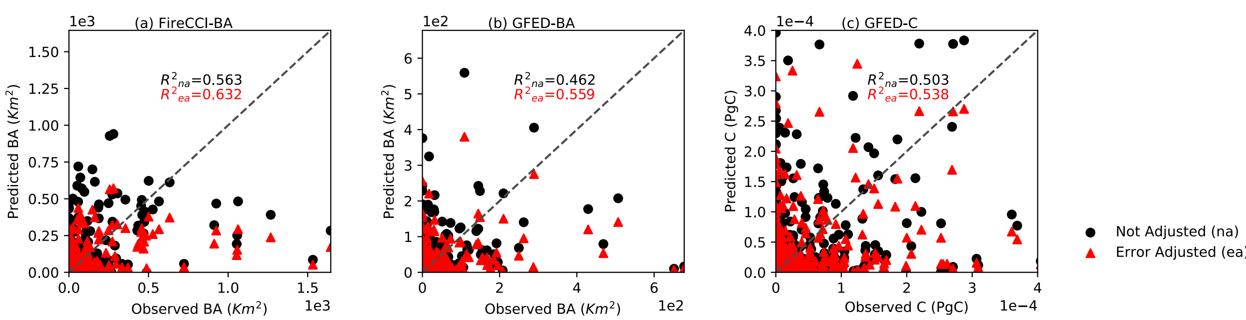

Figure S22 The scatter plots of observed and model predicted fire sizes. Model predictions–both error-adjusted (red triangle) and not-adjusted (black dot) predictions–are presented for (a) FireCCI burned area, (b) GFED burned area, and (c) GFED C emissions. The R^2_{na} and R^2_{ea} refer to the determination coefficients that without and with error adjustments, respectively.

References

Chuvieco, E., Pettinari, M. L., Lizundia-Loiola, J., Storm, T., and Padilla Parellada, M.: ESA Fire Climate Change InitiativeFire_cci: MODIS Fire_cci Burned Area Pixel product, version 5.13.1, https://doi.org/10.5285/58F00D8814064B79A0C49662AD3AF537, 2018.

Gelaro, R., McCarty, W., Suárez, M. J., Todling, R., Molod, A., Takacs, L., Randles, C. A., Darmenov, A., Bosilovich, M. G., Reichle, R., Wargan, K., Coy, L., Cullather, R., Draper, C., Akella, S., Buchard, V., Conaty, A., da Silva, A. M., Gu, W., Kim, G.-K., Koster, R., Lucchesi, R., Merkova, D., Nielsen, J. E., Partyka, G., Pawson, S., Putman, W., Rienecker, M., Schubert, S. D., Sienkiewicz, M., and Zhao, B.: The Modern-Era Retrospective Analysis for Research and Applications, Version 2MERRA-2, J. Climate, 30, 5419–5454, https://doi.org/10.1175/JCLI-D-16-0758.1, 2017.

Giglio, L., Boschetti, L., Roy, D. P., Humber, M. L., and Justice, C. O.: The Collection 6 MODIS burned area mapping algorithm and product, Remote Sensing of Environment, 217, 72–85, https://doi.org/10.1016/j.rse.2018.08.005, 2018.

Harris, I., Osborn, T. J., Jones, P., and Lister, D.: Version 4 of the CRU TS monthly high-resolution gridded multivariate climate dataset, Sci Data, 7, 109, https://doi.org/10.1038/s41597-020-0453-3, 2020.

Hugelius, G., Loisel, J., Chadburn, S., Jackson, R. B., Jones, M., MacDonald, G., Marushchak, M., Olefeldt, D., Packalen, M., Siewert, M. B., Treat, C., Turetsky, M., Voigt, C., and Yu, Z.: Large stocks of peatland carbon and nitrogen are vulnerable to permafrost thaw, PNAS, 117, 20438–20446, https://doi.org/10.1073/pnas.1916387117, 2020.

Klein Goldewijk, K., Beusen, A., Doelman, J., and Stehfest, E.: Anthropogenic land use estimates for the Holocene – HYDE 3.2, Earth System Science Data, 9, 927–953, https://doi.org/10.5194/essd-9-927-2017, 2017.

Madani, N. and Parazoo, N. C.: Global Monthly GPP from an Improved Light Use Efficiency Model, 1982-2016, ORNL DAAC, https://doi.org/10.3334/ORNLDAAC/1789, 2020.

Martens, B., Miralles, D. G., Lievens, H., van der Schalie, R., de Jeu, R. A. M., Fernández-Prieto, D., Beck, H. E., Dorigo, W. A., and Verhoest, N. E. C.: GLEAM v3: satellite-based land evaporation and root-zone soil moisture, Geoscientific Model Development, 10, 1903–1925, https://doi.org/10.5194/gmd-10-1903-2017, 2017.

Pinzon, J. E. and Tucker, C. J.: A non-stationary 1981-2012 AVHRR NDVI3g time series, Remote Sensing, 6, 6929–6960, https://doi.org/10.3390/rs6086929, 2014.

Randerson, J. T., Van der Werf, G. R., Giglio, L., Collatz, G. J., and Kasibhatla, P. S.: Global Fire Emissions Database, Version 4.1GFEDv4, ORNL DAAC, 2015.

Roy, D. P., Boschetti, L., Justice, C. O., and Ju, J.: The collection 5 MODIS burned area product — Global evaluation by comparison with the MODIS active fire product, Remote Sensing of Environment, 112, 3690–3707, https://doi.org/10.1016/j.rse.2008.05.013, 2008.

World Meteorological Organization: Guide to meteorological instruments and methods of observation, Secretariat of the World Meteorological Organization, 2008.